

Theory of Orbital Excitation and Resonant Inelastic X-ray Scattering in Manganites

Sumio Ishihara and Sadamichi Maekawa

Institute for Materials Research, Tohoku University, Sendai 980-8577 Japan

(May 7, 2018)

We study theoretically the collective orbital excitation named orbital wave in the orbital ordered manganites. The dispersion relation of the orbital wave is affected by the static spin structure through the coupling between spin and orbital degrees of freedom. As a probe to detect the dispersion relation, we propose two possible methods by utilizing resonant inelastic x-ray scattering. The transition probability of the orbital wave scattering is formulated, and the momentum and polarization dependences of the structure factor are calculated in several types of the orbital and spin structures. The elastic x-ray scattering in the L-edge case to observe the orbital ordering is also discussed.

71.10.-w, 71.90.+q, 75.90.+w, 78.70.Ck

I. INTRODUCTION

It is widely accepted that one of the important ingredients for the colossal magnetoresistance (CMR)¹⁻⁴ and various complex phenomena observed in perovskite manganites is the orbital degree of freedom in Mn³⁺ ion. Although the long range orbital ordering and its implications of the magnetic interaction were discussed long time ago,⁵⁻⁷ it has been recognized as a hidden degree of freedom, because the observation technique has been limited.⁸ Recently, the anomalous x-ray scattering (the resonant elastic x-ray scattering) shed light on the subject, that is, by using the method the orbital ordering in La_{0.5}Sr_{1.5}MnO₄ was directly observed.⁹ The alternate orbital alignment was confirmed by observation of the forbidden reflection originated from orbital dependence of the atomic scattering factor. In a moment, this experimental technique was recognized as a powerful probe to detect the orbital structure and applied to several undoped and doped manganites.¹⁰⁻¹² Through the intensive experimental and theoretical studies,¹³⁻¹⁵ it certainly uncovers roles of the orbital ordering on the electronic and lattice structures in manganites.

On the other hand, the dynamics of the orbital degree of freedom is still far from our understanding. In orbital ordered insulators, the collective excitation for the orbital degrees was first investigated by Cyrot *et al.* in the model where the orbital space was assumed to be isotropic.¹⁶ It was termed orbital wave in analogy with spin wave in a magnetic ordered state. For actual compounds, the present authors calculated the dispersion relation of

the orbital wave in the ($3d_{3x^2-r^2}/3d_{3y^2-r^2}$)-type orbital ordered state with A(layer)-type antiferromagnetic spin structure observed in LaMnO₃.¹⁷ When such a collective excitation in the orbital degree exists, it probably affects the thermodynamics and the dispersion relations of spin wave¹⁸ and phonon. Furthermore, the orbital excitation in the metallic phase seems to play an essential role in the transport and optical properties¹⁹ and CMR. As a probe to observe the orbital excitation, Inoue *et al.* theoretically examined the Raman scattering²⁰ where the excitation process is analogous of that in the magnon Raman scattering. In this method, the information of the Γ -point and the density of state of the orbital wave are obtained.

In this paper, we study theoretically the orbital wave in orbital ordered manganites and propose a method to observe it by the resonant inelastic x-ray scattering (RIXS). RIXS is rapidly developed through the recent progress of the synchrotron radiation source²¹ and is applied to several highly correlated electron systems.^{22,23} One of the advantages of this method on the subject is that the wave length of the x-ray is comparable to the lattice constant, unlike the conventional light. Therefore, the dispersion relation of the orbital wave in the wide range of the Brillouin zone is detectable by the method. The following two different processes in RIXS are proposed: the incident photon energy is tuned at 1) Mn³⁺ L-edge and 2) Mn³⁺ K-edge. We formulate the transition probability in both types of the scattering and the structure factor is calculated as a function of momentum and polarization in several orbital orderings.

In Sec. II, the dispersion relation of the orbital wave is calculated. We emphasize the strong correlation between the static spin structure and the orbital wave. In Sec. III, a mechanism to observe the orbital wave by RIXS is introduced. The general formulas of the scattering intensity and the numerical results of the structure factor are presented. Sec. V is devoted to the discussion and summary.

II. ORBITAL WAVE

In order to calculate the collective excitations in an orbital ordered insulator, we start with the Hamiltonian describing the low energy electronic structure in perovskite manganites. The cubic lattice consisting of Mn ions is considered and two e_g orbitals and a t_{2g} localized spin are introduced in each site. The Coulomb interactions

between e_g electrons (U, U', J) and the Hund coupling (J_H) between e_g and t_g spins are considered. Because the Coulomb interaction gives the largest energy among the relevant parameters, the Hamiltonian is derived by excluding the doubly occupied e_g states as follows,

$$\tilde{H}_{3d} = H_{e-e} + H_{e-t} + H_{t-t}. \quad (1)$$

The detailed derivation is presented in Ref. 17. The first term describes the interaction between nearest neighboring spins and orbitals in e_g orbitals,

$$H_{e-e} = -2J_1 \sum_{\langle ij \rangle} \left(\frac{3}{4} + \vec{S}_i \cdot \vec{S}_j \right) \left(\frac{1}{4} - \Psi_i^\dagger \hat{\tau}_{ij} \Psi_j \right) - 2J_2 \sum_{\langle ij \rangle} \left(\frac{1}{4} - \vec{S}_i \cdot \vec{S}_j \right) \left(\frac{3}{4} + \Psi_i^\dagger \hat{\tau}_{ij} \Psi_j + A_{ij} \right), \quad (2)$$

where a relation $U = U' + J$ is assumed with U, U' , and J being the intra- and inter-orbital Coulomb interactions and the exchange interaction in e_g orbitals, respectively. $J_1 = t_0^2/(U' - J)$ and $J_2 = t_0^2/(U' + J + 2J_H)$ with $J_1 > J_2$. $\Psi_i = [T_{iz}, T_{ix}]^t$ is a doublet of the orbital pseudo-spin operator: $\vec{T}_i = (1/2) \sum_{\sigma\gamma\gamma'} \vec{d}_{i\gamma\sigma}^\dagger (\vec{\sigma})_{\gamma\gamma'} \vec{d}_{i\gamma'\sigma}$ and $\vec{S}_{i\gamma\theta}$ is the spin operator with $S = 1/2$ for an e_g electron of orbital $\gamma\theta$. $\hat{\tau}_{ij}$ and A_{ij} are defined by

$$\hat{\tau}_{ii+l} = \frac{1}{2} \begin{pmatrix} 1 + \cos n_l \frac{2\pi}{3} & \sin n_l \frac{2\pi}{3} \\ \sin n_l \frac{2\pi}{3} & 1 - \cos n_l \frac{2\pi}{3} \end{pmatrix}, \quad (3)$$

and

$$A_{ij} = \Psi_i^\dagger M_{ij} n_j + H.c., \quad (4)$$

respectively, where $M_{ii+l} = (\cos n_l \frac{2\pi}{3}, -\sin n_l \frac{2\pi}{3})^t$ with $(n_x, n_y, n_z) = (1, 2, 3)$. The forms of $\hat{\tau}_{ij}$ and M_{ij} in the above are obtained by the Slater-Koster formulas for the transfer intensity $t_{ij}^{\gamma\gamma'}$ between site i with orbital γ and site j with γ' . It is worth noting that the orbital part of H_{e-e} is represented by T_z and T_x , since $t_{ij}^{\gamma\gamma'}$ is rewritten by the rotation matrix of the (T_z, T_x) -plane and the projection operator for $3d_{3z^2-r^2}$ orbital. The first term in Eq.(2) favors the ferromagnetic spin structure with the antiferro-type orbital ordering where two kinds of orbital sublattice exist. On the other hand, the second one favors the antiferromagnetic structure with the ferro-type orbital ordering where occupied orbital is uniform. The sum of the second and third terms in Eq.(1) is given by

$$H_{e-t} + H_{t-t} = -J_H \sum_{i\gamma\theta} \vec{S}_{t_{2g}i} \cdot \vec{S}_{i\gamma\theta} + J_{AF} \sum_{\langle ij \rangle} \vec{S}_{t_{2g}i} \cdot \vec{S}_{t_{2g}j}, \quad (5)$$

where J_{AF} is the antiferromagnetic superexchange interaction between nearest neighboring t_{2g} spins $\vec{S}_{t_{2g}i}$ with $S = 3/2$.

We first study the spin and orbital ordered structures at zero temperature in the mean field approximation. It is assumed that in each Mn site, one of the e_g orbitals is occupied by an electron. For both spin and orbital structures, we introduce four-types of the ordering: ferro-type (F-type) where spins or orbitals in all sites are parallel, and three kinds of antiferro-type, that is, layer-type (A-type), rod-type (C-type), and NaCl-type (G-type) where two kinds of spin or orbital sublattice exist. The rotating frame is introduced in the orbital space and the orbital state is described by an angle θ in the (T_z, T_x) -plane. In the scheme, the occupied orbital is represented by $|3d_{\gamma\theta}\rangle = \cos(\theta/2)|3d_{3z^2-r^2}\rangle - \sin(\theta/2)|3d_{x^2-y^2}\rangle$. As the order parameters, $\langle S_z \rangle$, $\langle S_{t_{2g}z} \rangle$ and $\langle T(\theta)_z \rangle = \cos\theta \langle T_z \rangle - \sin\theta \langle T_x \rangle$ with $\langle S_{t_{2g}z} \rangle = 3\langle S_z \rangle$ are introduced.

In Fig. 1, the mean field phase diagram is presented. A sequential change in the spin structure, that is, $F \rightarrow A \rightarrow C \rightarrow G$ with increasing J_2 and J_{AF} is caused by an enhancement of the antiferromagnetic interaction between spins. As for the orbital structure in the spin-F and spin-G phases, the orbital-G with $(\theta_A/\theta_B) = (\theta_A/\theta_A + \pi)$ for any θ_A and the orbital-C with $(\theta_A/\theta_B) = (\frac{\pi}{2}/\frac{3\pi}{2})$ are the mean field solutions^{7,24,25} with θ_A and θ_B being the angles in A and B orbital sublattices, respectively. In the orbital-G case, especially, the orbital space becomes isotropic in the (T_z, T_x) -plane, although the orbital part in the Hamiltonian Eq.(2) is not written by a simple vector product. This result is originated from 1) the relation,

$$\sum_{l=x,y,z} t_{ii+l}^{\gamma\gamma'} = \frac{3}{2} t_0 \delta_{\gamma\gamma'}, \quad (6)$$

due to the cubic symmetry of the lattice and 2) the cubic symmetry of the spin structure, that is, spin-F and -G. Because of these two conditions, the orbital part in H_{e-e} becomes diagonal and A_{ij} term vanishes. On the other hand, in spin-A and -C phases, the orbital state is uniquely determined. In spin-A, the orbital structure in the mean field theory is orbital-C and -G types with $(\theta_A/\theta_B) = (\theta_A/-\theta_A)$ where θ_A is determined by the equation $\theta_A = \cos^{-1}(2J_2/(5J_1 - J_2))$. It includes the $(\frac{1}{\sqrt{2}}(3d_{3z^2-r^2} - 3d_{x^2-y^2})/\frac{1}{\sqrt{2}}(3d_{3z^2-r^2} + 3d_{x^2-y^2}))$ orbital order at $J_2 = 0$ and $(3d_{z^2-x^2}/3d_{y^2-z^2})$ order at $J_2 = J_1$.^{7,24,25} The $(\theta_A/-\theta_A)$ -type orbital order in spin-A is consistent to the experimental results of the polarization dependence of the resonant elastic x-ray scattering,^{10,14} although the value of θ_A seems to be modified by the coupling with lattice. In spin-C, the mean field solution is orbital-G type with $(0/\pi)$ corresponding to the $(3d_{3z^2-r^2}/3d_{x^2-y^2})$. In both cases, the spin structure breaks the cubic symmetry in the system and causes the anisotropic interaction between nearest neighboring orbital pseudo-spins. This noticeable feature in the interplay between spin and orbital degrees clearly reflects on the dispersion relation of the orbital excitation, as will be discussed below.

We next study the orbital excitation in the orbital ordered states obtained in the mean field theory. The col-

lective excitations in the spin and orbital degrees of freedom are obtained by utilizing the conventional Holstein-Primakoff approximation.^{26–28} The dispersion relation in the spin-F case is shown in Fig. 2 where the types of the orbital order are chosen as $\theta_A = \pi n/6 = \theta_B - \pi$. The face-centered cubic (fcc) lattice is adopted as a unit cell which includes two Mn ions. The analytic form of the dispersion relation and the eigen-operator are given by

$$\omega_k^{(\pm)} = 3\sqrt{\alpha(\alpha \pm \beta)}, \quad (7)$$

with

$$\alpha = -2J_1 \frac{1}{3} \sum_{l=x,y,z} (\tau_{ii+l})_{11}, \quad (8)$$

$$\beta = 2J_1 \frac{1}{3} \sum_{l=x,y,z} \cos(ak_l) (\tau_{ii+l})_{22}, \quad (9)$$

and

$$\begin{aligned} \phi^{(\pm)} = & \cosh \theta_k^{(\pm)} \frac{1}{\sqrt{2}} (a_k \pm b_k) \\ & + \sinh \theta_k^{(\pm)} \frac{1}{\sqrt{2}} (a_{-k}^\dagger \pm b_{-k}^\dagger), \end{aligned} \quad (10)$$

with $2\theta_k^{(\pm)} = \tanh^{-1}(\pm\beta/(2\alpha \pm \beta))$, respectively. a_k and b_k are the Fourier transform of the Holstein-Primakoff bosons for the two orbital sublattices defined in the rotating frame. The (+)-mode is the gapless mode and its eigen-operator includes the components $T_{Ax} - T_{Bx}$ and $T_{Ay} + T_{By}$. At the Γ -point, the x -component of the staggered orbital order parameter $\langle (\sum_{i \in A} T_{ix} - \sum_{i \in B} T_{ix})^2 \rangle$ diverges since the orbital space is isotropic. With increasing θ_A , the stiffness of the orbital wave along the $\Gamma - X$ direction becomes weak and at $\theta_A = 4\pi/6$ ($3d_{3x^2-r^2}/3d_{y^2-z^2}$) it becomes flat. It is originated from $(\tau_{ii+x})_{22} = 0$ in Eq.(9) since the electron transfer between $3d_{y^2-z^2}$ orbitals along the x direction vanishes. The similar gapless mode and the changes of the stiffness with changing types of the orbitals are also obtained in the spin-G case. The isotropic nature in the orbital space in spin-F case is seen by the Fourier transforming of the Hamiltonian (Eq.(2)) as

$$H_{e-e} = -2J_1 \sum_{\vec{k}} \left(\frac{3}{2} - \sum_{l=z,x} \tilde{T}_l(\vec{k}) \tilde{\tau}_l(\vec{k}) \tilde{T}_l(\vec{k}) \right), \quad (11)$$

in the spin-F case.¹⁹ $\tilde{T}_l(\vec{k})$ is the orbital pseudo-spin operator which diagonalizes the matrix $\hat{\tau}_{ij}$ and

$$\begin{aligned} \tilde{\tau}_l(\vec{k}) = & 2((c_x + c_y + c_z) \\ & \pm (c_x^2 + c_y^2 + c_z^2 - c_x c_y - c_y c_z - c_z c_x)^{1/2}), \end{aligned} \quad (12)$$

where + and - are for $l = z$ and x , respectively, and $c_l = \cos(ak_l)$. At the Γ - and R -points, $\tilde{\tau}_x = \tilde{\tau}_z$, so that the orbital system becomes isotropic.

The orbital excitation in the spin-A case is qualitatively different from that in the spin-F case as shown in Fig. 3. The unit cell with four Mn ions is adopted, so that there exist four modes. Two of them have the dispersion relations,

$$\omega_k^{(+\pm)} = \frac{1}{2} \sqrt{(2\alpha_{xy} + \alpha_{zz}) [2(\alpha_{xy} + \beta_{xy}) + (\alpha_{zz} \pm \beta_{zz})]}, \quad (13)$$

and the other two $\omega^{(-\pm)}$ are given by replacing $(\alpha_{xy} + \beta_{xy})$ in Eq.(13) by $(\alpha_{xy} - \beta_{xy})$. Here,

$$\begin{aligned} \alpha_{lm} = & -2J_1 \left(\frac{3}{4} + K_{lm} \right) (\tau_{lm})_{11} \\ & + 2J_2 \left(\frac{1}{4} - K_{lm} \right) ((\tau_{lm})_{11} + 2(M_{lm})_1), \end{aligned} \quad (14)$$

and

$$\beta_{lm} = \left[2J_1 \left(\frac{3}{4} + K_{lm} \right) - 2J_2 \left(\frac{1}{4} - K_{lm} \right) \right] (\gamma_{lm})_{22}, \quad (15)$$

for $(lm) = (xy)$ or (zz) . In these formulas, $A_{lm} = (1/2) \sum_{n=l,m} A_{ii+n}$ for $A = \tau$ and M , $\gamma_{lm} = (1/2) \sum_{n=l,m} \tau_{ii+n} \cos(ak_n)$ and K_{lm} is the spin correlation function given by $K_{lm} = (1/2) \sum_{n=l,m} \langle (S_i)_z (S_{i+n})_z \rangle$. Among the four modes, $(++)$ -mode is the lowest one and its eigen-operator is expressed as

$$\begin{aligned} \phi_k^{(++)} = & \cosh \theta_k^{(++)} \frac{1}{2} (a_{1k} + a_{2k} + b_{1k} + b_{2k}) \\ & + \sinh \theta_k^{(++)} \frac{1}{2} (a_{1-k}^\dagger + a_{2-k}^\dagger + b_{1-k}^\dagger + b_{2-k}^\dagger), \end{aligned} \quad (16)$$

where the subscripts 1 and 2 imply the spin sublattices. The operator includes the components $T_{A_1x} + T_{A_2x} - T_{B_1x} - T_{B_2x}$ and $T_{A_1y} + T_{A_2y} + T_{B_1y} + T_{B_2y}$ and it corresponds to $(+)$ -mode in the spin-F case. At the Γ -point, the energy is obtained as

$$\omega_{k=\Gamma}^{(++)} = \frac{1}{2} \sqrt{(2\alpha_{xy} + \alpha_{zz}) A^{(++)}}, \quad (17)$$

with

$$\begin{aligned} A^{(++)} = & \sum_{(lm)=(xy),(zz)} z_{lm} \\ & \times \left\{ \left[-2J_1 \left(\frac{3}{4} + K_{lm} \right) + 2J_2 \left(\frac{1}{4} - K_{lm} \right) \right] \right. \\ & \times ((\tau_{lm})_{11} - (\tau_{lm})_{22}) \\ & \left. + 2J_2 \left(\frac{1}{4} - K_{lm} \right) 2(M_{lm})_1 \right\}, \end{aligned} \quad (18)$$

where $z_{xy} = 2$ and $z_{zz} = 1$. This mode is gapful in contrast with the spin-F case. The right hand side in Eq. (18) is represented by a product of the spin correlation function and the anisotropic transfer intensity.

Therefore, the origin of the gap is attributed to the fact: 1) The orbital space is anisotropic, i.e., $(\tau)_{11} \neq (\tau)_{22}$ and $A_{ij} \neq 0$, which originate from the anisotropic transfer intensity $t_{ij}^{\gamma\gamma'} \neq \delta_{\gamma\gamma'}$. 2) The spin correlation functions in the xy plane and in the z direction are different ($K_{xy} \neq K_{zz}$). The gapful excitation is also obtained in the spin-C case. It is concluded that the anisotropic spin structure breaks the cubic symmetry in the system and causes the anisotropy in the orbital space, which causes the gap in the orbital wave.

III. RESONANT INELASTIC X-RAY SCATTERING

In this section, we propose a method to detect the orbital wave by RIXS. The following two excitation processes are considered: 1) the incident energy is tuned at Mn³⁺ L-edge and 2) at Mn³⁺ K-edge. Hereafter, the former and latter processes are termed L-edge and K-edge cases, respectively. The schematic processes are presented in Fig. 4. In the L-edge case, the incident x-ray excites an electron from Mn 2*p* orbital to the unoccupied Mn 3*d* orbital, and then one of the 3*d* electrons fills the core hole with emitting the x-ray. When the occupied orbitals are different between the initial and final states, the orbital excitation is brought about and the excitation propagates through the interaction between the nearest neighboring pseudo-spins. This process is denoted by,

$$|3d_{\gamma}^1\rangle + h\nu \rightarrow |3d_{\gamma}^1 3d_{\gamma'}^1 \underline{2p}\rangle \rightarrow |3d_{\gamma''}^1\rangle + h\nu' , \quad (19)$$

where $\underline{2p}$ implies that one hole occupies the Mn 2*p* orbital. In the K-edge case, the excitation occurs through the screening process. At first, the incident x-ray excites an electron from Mn 1*s* orbital to the unoccupied Mn 4*p* one at i site. At the time, an O 2*p* electron comes from one of the nearest neighbor oxygen sites to the Mn site and screens the potential due to the Mn 1*s* core hole. This screening process is confirmed by the theoretical calculation in the small cluster and the x-ray absorption spectroscopy experiments.^{13,29,30} Due to the hybridization between the O 2*p* and Mn 3*d* orbitals, this state strongly mixes with the state where an e_g orbital in one of the nearest neighbor Mn sites (j site) is empty. When the electron in the 4*p* orbital is relaxed to the 1*s* orbital with emitting x-ray, one of the 3*d* electrons in i site comes back to j site and the orbital excitation is brought about. This is represented by

$$\begin{aligned} |3d_{i\gamma_i}^1 3d_{j\gamma_j}^1\rangle + h\nu &\rightarrow |3d_{i\gamma_i}^1 3d_{i\gamma'_i}^1 \underline{1s_i} 4p_i^1\rangle \\ &\rightarrow |3d_{i\gamma'_i}^1 3d_{j\gamma'_j}^1\rangle + h\nu' , \end{aligned} \quad (20)$$

where O 2*p* states is integrated out. Although this excitation process is similar to that of the Raman scattering due to the orbital wave,²⁰ the current operators are different between the two. Furthermore, in the Raman scattering for the conventional light, the polarization of the light

determines the direction between i and j sites, unlike in the present case. In the case of manganites, the charge transfer from the nearest neighboring Mn sites occurs more easily than cuprates and nickelates, since the intra-site Coulomb interaction (U) is smaller and the energy gain of the Hund coupling in the intermediate states ($3d^5$ states) is larger in the present case.³¹ In the L-edge case the one-orbital wave excitation is only brought about. On the other hand, in the K-edge case, both one- and two-orbital wave excitations occur.

A. L-edge case

The transition probability of RIXS for the orbital wave is calculated in the electron-photon coupled system with the Hamiltonian,

$$H = H_{ele} + H_{ph} + H_{e-p} . \quad (21)$$

The first term is the electronic one for the Mn 3*d* and Mn 2*p* orbitals which includes the following three terms:

$$H_{ele} = H_{3d} + H_{2p} + H_{3d-2p} , \quad (22)$$

with

$$\begin{aligned} H_{3d} &= \varepsilon_d \sum_{i\gamma\theta\sigma} d_{i\gamma\theta\sigma}^\dagger d_{i\gamma\theta\sigma} + \sum_{\langle ij \rangle \gamma\gamma'\sigma} t_{ij}^{\gamma\gamma'} d_{i\gamma\sigma}^\dagger d_{j\gamma'\sigma} \\ &+ U \sum_{i\gamma\theta} n_i(3d_{\gamma\theta\uparrow}) n_i(3d_{\gamma\theta\downarrow}) \\ &+ U' \sum_{i\sigma\sigma'\gamma\theta} n_i(3d_{\gamma\theta+\sigma}) n_i(3d_{\gamma\theta-\sigma'}) \\ &+ J \sum_{i\sigma\sigma'\gamma\theta} d_{i\gamma\theta+\sigma}^\dagger d_{i\gamma\theta-\sigma'}^\dagger d_{i\gamma\theta+\sigma'} d_{i\gamma\theta-\sigma} \\ &+ H_{e-t} + H_{t-t} , \end{aligned} \quad (23)$$

and

$$\begin{aligned} H_{2p} + H_{3d-2p} &= \varepsilon_p \sum_{i\gamma\sigma} p_{i\gamma\sigma}^\dagger p_{i\gamma\sigma} \\ &+ \sum_{i\gamma\theta\gamma} V(3d_{\gamma\theta}, 2p_{\gamma}) n_i(3d_{\gamma\theta}) n_{hi}(2p_{\gamma}) . \end{aligned} \quad (24)$$

$n_i(3d_{\gamma\sigma})$ and $n_{hi}(2p_{\gamma\sigma})$ are the number operators for Mn 3*d* electron and Mn 2*p* hole, respectively. $V(3d_{\gamma\theta}, 2p_{\gamma})$ is the Coulomb interaction between Mn 3*d* and 2*p* and is given by $V(3d_{\gamma\theta}, 2p_{\gamma}) = F_0(3d, 2p) - 4F_2(3d, 2p) \cos\left(\theta + n_{\gamma} \frac{2\pi}{3}\right)$.¹³ The second and third terms in Eq. (21) describe the photon part and electron-photon interaction, respectively, and a sum of them is given by

$$\begin{aligned} H_{ph} + H_{e-p} &= \sum_{k\lambda} \omega_k \left(a_{k\lambda}^\dagger a_{k\lambda} + \frac{1}{2} \right) , \\ &- \sum_{k\lambda} \sqrt{\frac{2\pi}{\Omega}} \frac{1}{\sqrt{\omega_k}} \vec{j}_k \cdot \vec{e}_{k\lambda} \left(e^{-i\omega_k t} a_{k\lambda} + e^{i\omega_k t} a_{k\lambda}^\dagger \right) , \end{aligned} \quad (25)$$

where $a_{\vec{k}\lambda}^\dagger$ is the photon creation operator with momentum \vec{k} and polarization λ . In the L-edge case, the current operator describes the $2p \rightarrow 3d$ transition as

$$(\vec{j}_k)_\alpha = \sum_{i\gamma\theta\sigma} A_{i\gamma\theta\alpha}^{(L)} a_{i\gamma\theta\sigma}^\dagger p_{i\alpha\sigma} e^{i\vec{k}\cdot\vec{R}_i} + H.c. \quad (26)$$

The coupling constant depends on the polarization and the orbital as follows,

$$A_{i\gamma\theta\alpha}^{(L)} = A_0 \cos\left(\frac{\theta}{2} + n_\alpha \frac{2\pi}{3}\right). \quad (27)$$

with $(n_x, n_y, n_z) = (1, 2, 3)$. A_0 is a constant part defined by

$$A_0 = i \frac{e}{m} \left(\frac{3\sqrt{5}}{4\pi} \right) \left\langle \frac{-6z^2 x^2}{r^5} + \frac{x^2 z^2}{r^4} \nabla_r - \frac{x^4}{r^4} \nabla_r \right\rangle \quad (28)$$

where $\langle A \rangle = \int dr R_{2p}(r) A R_{3d}(r)$.

Being based on the Hamiltonian, the scattering matrix for the orbital wave is derived. The initial and final states are described by \tilde{H}_{3d} (Eq.(1)) where the orbital wave is the eigen-mode. The intermediate state is described by the single site term in H_{ele} (Eq.(22)) and the inter-site effects are neglected. The explicit form of the inelastic part of the scattering matrix is obtained as

$$\begin{aligned} (S)_{fi} &= -2\pi i \delta(E_f - E_i) \\ &\times \frac{2\pi}{\Omega} \sum_{k_1 k_2 \lambda_1 \lambda_2} \frac{1}{\sqrt{\omega_{k_1} \omega_{k_2}}} \sum_{\alpha i} (e_{k_1 \lambda_1})_\alpha (e_{k_2 \lambda_2})_\alpha \\ &\times e^{i(\omega_{k_1} - \omega_{k_2})t - i(\vec{k}_1 - \vec{k}_2) \cdot \vec{R}_i} I_{i\alpha} D. \end{aligned} \quad (29)$$

$E_{i(f)}$ is the energy at the initial (final) state in the electron-photon system. In Appendix A, we discuss the elastic part which is a probe to detect the orbital ordering. In the above formula, the orbital excitation by x-ray is represented by the operator,

$$I_{i\alpha} = (A_{ia\alpha}^{(L)*} A_{ib\alpha}^{(L)} T_{i-} + A_{ib\alpha}^{(L)*} A_{ia\alpha}^{(L)} T_{i+}), \quad (30)$$

where subscript $a(b)$ indicates the occupied (unoccupied) $3d$ orbital at site i . D is the energy denominator in the perturbation given by

$$D = -\frac{3}{2} E^{(t)-1} + \frac{1}{2} E^{(s)-1}. \quad (31)$$

Two terms correspond to the different intermediate states where two electrons occupy the different e_g orbital with the triplet and singlet spin states, respectively (see Appendix A). It is mentioned that when the wave function is chosen to be real, $I_{i\alpha}$ in Eq.(30) is expressed by T_x , and it is in contrast to the neutron scattering where both S_x and S_y appear in the scattering matrix. This remarkable feature brings about the selection rule between the reciprocal lattice vector and the mode of the orbital wave as we will show later. The transition probability

is obtained by the conventional golden rule. By rewriting the pseudo-spin operator in Eq.(30) by the Holstein-Primakoff bosons, we obtain the transition probability in the L-edge case:

$$\begin{aligned} W &= C \sum_{Gq\mu} |F_{\mu\alpha}(\vec{q}, \vec{G})|^2 \\ &\times (\delta_{\vec{k}_1 - \vec{k}_2 + \vec{q} + \vec{G}} \delta(\omega + \omega_q^{(\mu)})(1 + n_q^{(\mu)}) \\ &+ \delta_{\vec{k}_1 - \vec{k}_2 - \vec{q} + \vec{G}} \delta(\omega - \omega_q^{(\mu)}) n_q^{(\mu)}), \end{aligned} \quad (32)$$

with $C = (2\pi/\Omega \sqrt{\omega_{k_1} \omega_{k_2}})^2$. $n_q^{(\mu)}$ is the number of the orbital wave of mode μ and \vec{G} is the reciprocal lattice vector. Since the one orbital wave process is possible in the present case, the transition probability shows a similar form to that for the one magnon neutron scattering. Difference in the present case from the magnon scattering reflects on the generalized structure factor:

$$F_{\mu\alpha}(\vec{q}, \vec{G}) = D \sum_{\nu} A_{\nu a\alpha}^{(L)*} A_{\nu b\alpha}^{(L)} (V_{\nu\mu}(\vec{q}) + W_{\nu\mu}(\vec{q})) e^{i\vec{G} \cdot \vec{r}_\nu}, \quad (33)$$

where $V_{\nu\mu}(\vec{q})$ and $W_{\nu\mu}(\vec{q})$ are the coefficients in the Bogolyubov transformation which connect the operator for the ν -th ion to that for the μ -th eigen mode as

$$a_{\nu q} = \sum_{m\mu} V_{\nu\mu}(\vec{q}) \alpha_{m q} + W_{\nu\mu}(\vec{q}) \alpha_{\mu - q}^\dagger. \quad (34)$$

It is noticeable that in the above formula, \vec{G} , \vec{q} , and α -dependence of the structure factor is mainly dominated by the factors $e^{i\vec{G} \cdot \vec{r}_\nu}$, $V_{\nu\mu}(\vec{q}) + W_{\nu\mu}(\vec{q})$ and $A_{\nu\gamma\alpha}^{(L)}$, respectively.

In Fig. 5, numerical results of the structure factor for the spin-F case is presented. The orbital state is chosen as $(\theta_A/\theta_B) = (\frac{\pi}{2}/\frac{\pi}{2} + \pi)$. $\vec{G} = (h, k, l)$ for the fcc lattice is chosen as $h+k+l = \text{even}$ (Fig. 5(a)) and odd (Fig. 5(b)), respectively. It is clear that the (+)- and (-)-modes are observed separately in the odd and even cases, and their weights are proportional to $(\cosh \theta_q^{(+)} + \sinh \theta_q^{(+)})^2$ and $(\cosh \theta_q^{(-)} + \sinh \theta_q^{(-)})^2$, respectively. This selection rule is originated from the following facts: 1) when the wave functions of the e_g orbitals are chosen to be real, the scattering matrix in Eq.(29) and (30) is represented by T_x , 2) the absolute value of the coupling constants $|A_{\nu a\alpha}^{(L)} A_{\nu b\alpha}^{(L)}|^2$ in the two sublattices is the same in the orbital order $(\theta_A/\theta_A + \pi)$, 3) the relative motion of the pseudo-spin in (+)- and (-)-modes is opposite, and 4) there exists the factor $e^{i\vec{G} \cdot \vec{r}_\nu}$. It is shown that this selection rule does not depend on the phase of the wave functions of the e_g orbitals. It is highly in contrast to the case of one magnon neutron scattering where the correlation function of S_y breaks the selection rule and the (+)- and (-)-modes are also observed in the $h+k+l = \text{even}$ and odd cases with weights of $(\cosh \theta_q^{(+)} - \sinh \theta_q^{(+)})^2$

and $(\cosh \theta_q^{(-)} - \sinh \theta_q^{(-)})^2$, respectively. The intensity of the structure factor monotonically increases with decreasing the energy and it diverges at the Γ -point. This \vec{q} -dependence comes from $V_{\nu\mu}(\vec{q}) + W_{\nu\mu}(\vec{q})$ which is proportional to $(\cosh \theta_q^{(\mu)} + \sinh \theta_q^{(\mu)})^2$. The divergence at the Γ -point is originated from the divergence of the x component of the staggered orbital order parameter due to the rotational symmetry in the (T_z, T_x) -plane. In the figure, the intensity in the z -polarization is larger than that in the x -polarization and the ratio does not depend on \vec{q} . It is interpreted that the orbital order is close to $(3d_{3x^2-r^2}/3d_{y^2-z^2})$ where $A_{y^2-z^2, x}^{(L)}$ is zero due to the symmetry. In Fig. 6, the structure factor in the spin-A case with the x -polarization is shown. The four modes of the orbital wave, that is, $(+\pm)$ - and $(-\pm)$ -modes are mainly observed for $h+k=\text{odd}$, $l=\text{odd}$ (even), and $h+k=\text{even}$, $l=\text{odd}$ (even), respectively. Strictly speaking, this selection rule is satisfied in the case of $J_2 = 0$ and in general, $(++)$ - and $(--)$ -modes and $(+-)$ - and $(-+)$ -modes are mixed each other. The intensity does not diverge at the Γ -point, unlike that in the spin-F case, since the rotational symmetry in the orbital space is broken by the anisotropic spin structure. The intensity is larger in the presented z -polarization case in comparison with that in the x -polarization one, although the results in the x -polarization are only shown in the figure. It is attributed to the type of the orbital order which is close to $(3d_{3x^2-r^2}/3d_{y^2-z^2})$ rather than $(3d_{3z^2-r^2}/3d_{x^2-y^2})$.

B. K-edge case

In the K-edge case, we derive the effective Hamiltonian for the electron-photon system and calculate the transition probability by using the Hamiltonian. The electronic part of the Hamiltonian, where Mn $3d$, $4p$ and $1s$ orbitals are introduced, is given by¹³

$$H_{ele} = H_0 + H_{3d} + H_{3d-4p} + H_{1s-3d} + H_{1s-4p}, \quad (35)$$

with

$$H_0 = \varepsilon_P \sum_{i\gamma\sigma} P_{i\gamma\sigma}^\dagger P_{i\gamma\sigma} + \varepsilon_s \sum_{i\sigma} s_{i\sigma}^\dagger s_{i\sigma}, \quad (36)$$

where $s_{i\sigma}$ and $P_{i\gamma\sigma}$ are the annihilation operator of Mn $1s$ and $4p$ electron with spin σ and orbital γ , respectively. The last three terms in Eq.(35) describe the Coulomb interactions:

$$\begin{aligned} & H_{3d-4p} + H_{1s-3d} + H_{1s-4p} \\ &= \sum_{i\gamma\theta} V(3d_{\gamma\theta}, 4p_\gamma) n_i(3d_{\gamma\theta}) n_i(4p_\gamma) \\ &+ \sum_{i\gamma\theta} V(3d, 1s) n_i(3d_{\gamma\theta}) n_{hi}(1s) \\ &+ \sum_{i\gamma} V(4p, 1s) n_i(4p_\gamma) n_{hi}(1s). \end{aligned} \quad (37)$$

In the present case, the current operator in H_{e-p} describes the $1s \rightarrow 4p$ transition as¹³

$$(\vec{j}_k)_\alpha = \sum_{i\sigma} A^{(K)} P_{i\alpha\sigma}^\dagger s_{i\sigma} e^{i\vec{k}\cdot\vec{R}_i} + H.c. \quad (38)$$

$A^{(K)}$ is the coupling constant defined by

$$A^{(K)} = \frac{e}{m} \int d\vec{r} \phi_{4p\alpha}^*(\vec{r}) (-i\nabla_\alpha) \phi_{1s}(\vec{r}), \quad (39)$$

which is derived by the dipole approximation and does not depend on the polarization α .

The scattering process in the K-edge case includes the electron transfer as shown in Fig. 4(b) and is derived by the fourth order process with respect to H_{e-p} and H_t (the transfer term in H_{3d} (Eq.(23)). Therefore, in order to avoid complications due to the higher order perturbation, we derive the effective Hamiltonian by the following procedure. In the initial and final states of the scattering, the energy of the doubly occupied e_g state is higher than that of the singly occupied one by the order of the Coulomb interaction between $3d$ electrons. In the intermediate state, on the other hand, due to the screening effects, the energy of the singly occupied state is higher than that of the doubly occupied one by the order of (the screening potential)-(the Coulomb interactions between $3d$ electrons and $3d$ and $4p$ electrons). By excluding these two states which have the higher energy eigen values, we derive the effective Hamiltonian by the second order perturbational calculation of H_t and/or H_{e-p} as follows,

$$\tilde{H} = H_{e-e} + H_{core} + \tilde{H}_{e-p} + H_{ph}. \quad (40)$$

The detailed derivation is presented in Appendix B. The first term was introduced in Eq.(2) and the second term describes the electronic states where the $1s$ core hole and the $4p$ electron always exist. The third term is recognized as the effective electron-photon interaction given by

$$\begin{aligned} \tilde{H}_{e-p} &= -\sqrt{\frac{2\pi}{\Omega}} \sum_{i\delta} \sum_{mk\lambda\alpha} \sum_{\gamma\gamma'\gamma''\sigma\sigma'} \frac{1}{\sqrt{\omega_k}} t_{ii+\delta}^{\gamma\gamma''} \Gamma_{\gamma\alpha}^{(m)} \\ &\times (P_m d_{i\gamma'\sigma'}^\dagger n_i(3d_{\gamma\sigma}) d_{i+\delta\gamma''\sigma'}) \\ &\times j_{i\alpha k} a_{k\lambda}(e_{k\lambda})_\alpha e^{-i\omega_k t} + H.c. \end{aligned} \quad (41)$$

It implies the electron excitation from $1s$ to $4p$ accompanied with the electron transfer from $i + \delta$ site to i site, where the operator P_m projects out the m -th doubly occupied state. $\Gamma_{\gamma\alpha}^{(m)}$ is the energy denominator derived in the perturbational calculation (Eq.(B1)) and $(j_{ik})_\alpha$ is the i -th component in Eq.(38).

The scattering matrix is calculated by the perturbation of the effective interaction \tilde{H}_{e-p} and is given by

$$\begin{aligned} (S)_{fi} &= -2\pi i \delta(E_f - E_i) \\ &\times \frac{2\pi}{\Omega} \sum_{k_1 k_2 \lambda_1 \lambda_2 \alpha} \frac{1}{\sqrt{\omega_{k_1} \omega_{k_2}}} \sum_{i\sigma} (e_{k_1 \lambda_1})_\alpha (e_{k_2 \lambda_2})_\alpha \end{aligned} \quad (42)$$

$$\begin{aligned} & \times e^{i(\omega_{k_1} - \omega_{k_2})t - i(\vec{k}_1 - \vec{k}_2) \cdot \vec{R}_i} \\ & \times |A^{(K)}|^2 \sum_{\delta} \sum_m I_{i\delta\alpha}^{(m)} D_{\alpha}^{(m)}. \end{aligned} \quad (43)$$

$D_{\alpha}^{(m)}$ and $I_{i\delta\alpha}^{(m)}$ are defined in Appendix B. $I_{i\delta\alpha}^{(m)}$ is the main part of the formula and is expressed by the spin and orbital pseudo-spin operators in i and its nearest neighbor $i + \delta$ sites. It is noticeable that $I_{i\delta\alpha}^{(m)}$ is described by T_x and T_z (see Appendix B), as well as that in the L-edge case in Eq.(30). It describes changes of the spin and orbital states in these sites. The scattering processes, where the one and two orbital waves are concerned, are included in $I_{i\delta\alpha}^{(m)}$ and these processes occur in the same order. This is in contrast to the conventional magnon Raman scattering where the two magnon sector is dominant. This is attributed the fact that $t_{ij}^{\gamma\gamma'} \neq \delta_{\gamma\gamma'}$. Therefore, we consider the processes for the one orbital wave excitation in $I_{i\delta\alpha}^{(m)}$ schematically shown in Fig. 7. In this approximation, the transition probability is obtained as the same form as Eq. (32) with the structure factor replaced by

$$\begin{aligned} F_{\mu\alpha}(\vec{q}, \vec{G}) &= 2 \sum_{\nu m} D_{\alpha}^{(m)} e^{i\vec{G} \cdot \vec{r}_{\nu}} |A^{(K)}|^2 \\ & \times \sum_{\nu'} \left((V_{\nu\mu}(\vec{q}) + W_{\nu\mu}(\vec{q})) C_{\nu\nu'}^{(m)} \right. \\ & \left. + e^{i\vec{q} \cdot (\vec{r}_{\nu} - \vec{r}_{\nu'})} (V_{\nu'\mu}(\vec{q}) + W_{\nu'\mu}(\vec{q})) B_{\nu\nu'}^{(m)} \right). \end{aligned} \quad (44)$$

The index ν' indicates one of the nearest neighboring Mn ions of the ν -th ion and $B_{\nu\nu'}^{(m)}$ and $C_{\nu\nu'}^{(m)}$ are represented by the spin correlation function defined in Appendix B. The two terms in the parenthesis in Eq. (44) corresponds to the orbital excitation in ν site and its nearest neighboring ν' site, respectively. As a result, the factor $e^{i\vec{q} \cdot (\vec{r}_{\nu} - \vec{r}_{\nu'})}$ gives the additional \vec{q} -dependence in the structure factor.

In Fig. 8, the numerical results of the structure factor in the spin-F case are presented. The parameter values are chosen as $w_0/t_0 = 0.5$, $W/t_0 = -6$, $\tilde{U}/t_0 = 5$, $J/t_0 = 1.0$, and $\Gamma/t_0 = 0.5$ (see Appendix B), although the qualitative results do not depend on the parameter values. $h + k + l = \text{odd}$ and even cases mainly correspond to (+)- and (-)-modes, respectively, although the both intensities are strongly mixed each other. The \vec{q} -dependence of the intensity is not monotonic, unlike that in the L-edge case shown in Fig. 5. Especially, around the Γ -point, the intensity gradually decreases and becomes zero at the point. This is attributed to the following unique excitation process in the K-edge case. With using the relations $\sum_l t_{ii+l}^{aa} t_{ii+l}^{ba} = 0$ and $\sum_l t_{ii+l}^{bb} t_{ii+l}^{ba} = 0$, in the uniform spin structure, $\sum_{\nu'} C_{\nu\nu'} = 0$ and $\sum_{\nu'} B_{\nu\nu'} = 0$ are derived. These relations suppress the divergence of the factor $V_{\mu\nu}(\vec{q}) + W_{\mu\nu}(\vec{q})$ at the Γ -point in Eq. (44), so that the intensity becomes zero at the point. It implies that at the Γ -point the several orbital excitation processes by x-ray are canceled out each other. The other

characteristic \vec{q} -dependences of the intensity, such as, no intensity along the $\Gamma - L$ direction, are interpreted by the factor $e^{i\vec{q} \cdot (\vec{r}_{\nu} - \vec{r}_{\nu'})}$. The polarization dependence of the intensity comes from the Coulomb interaction $V(3d_{\gamma}, 4p_{\alpha})$ included in $\Gamma_{\gamma\alpha}^{(m)}$, although it is not remarkable in comparison with that in the L-edge case (Fig. 9). Around the X -point, the slightly larger intensity is shown in the x -polarized case in comparison with that in the z -polarized one and it is interpreted as follows. In the present orbital order, a dominant excitation process around X -point is that in Fig. 5(b), where the orbital states in i and j sites are $\theta = \frac{\pi}{2} + \pi$ and $\frac{\pi}{2}$, respectively. Since the orbital at the i -site, that is, $\frac{1}{\sqrt{2}}(3d_{3z^2-r^2} + 3d_{x^2-y^2})$, shrinks in x -direction, the $1s \rightarrow 4p_x$ excitation shows a larger intensity than that of $1s \rightarrow 4p_{y(z)}$ excitation due to the Coulomb interaction. Therefore, the intensity is slightly larger in the x -polarized case. In Fig. 10, the results in the spin-A case with the x -polarization are presented. The relation between the reciprocal lattice vector and the four excitation modes is the same as that in the L-edge case. However, the two modes are mixed and the mixing becomes remarkable around the M -point due to the factor $e^{i\vec{q} \cdot (\vec{r}_{\nu} - \vec{r}_{\nu'})}$. The intensity of the structure factor does not show a strong polarization dependence of x-ray in comparison with that in the L-edge case, since the polarization dependence is originated from that in $\Gamma_{\gamma\alpha}^{(m)}$ as explained above.

IV. SUMMARY AND DISCUSSION

In this paper, we study the orbital excitation in the orbital ordered manganites and the method to observe the excitation by using the resonant inelastic x-ray scattering. At first, we emphasize the noticeable correlation between the static spin structure and the orbital excitation. The anisotropic spin ordering brings about the anisotropy in the orbital space and causes the gap in the orbital excitation. In this case, the interaction between spin wave and phonon seems to be weak, since the gap in the orbital excitation is of the order of t_0^2/U . This situation is expected to be realized in LaMnO₃ where the orbital ordered temperature accompanied with the structural phase transition occurs $T_O = 780K$ and the A-type antiferromagnetism is realized at $T_N = 140K$.¹⁰ Although the coupling with the lattice contributes to the gap, it is predicted that the nature of the orbital excitation is changed at T_N and below the temperature the gap becomes more remarkable. On the other hand, in the spin-F case, the orbital excitation becomes gapless and the low lying excitation affects the thermodynamic and transport properties. In this case, the dispersion relation is modified by the interaction between spin wave and phonon. The specific heat which is proportional to T^3 is derived by the linear dispersion of the orbital wave, which is distinguished from the contribution from the ferromagnetic spin wave. The possible candi-

date, where the gapless excitation is anticipated, is the ferromagnetic insulating phase realized in the low hole doped manganites, where the superexchange interaction between e_g orbitals dominates the ferromagnetic interaction rather than the double exchange one.^{24,11} Especially, in $\text{La}_{0.88}\text{Sr}_{0.12}\text{MnO}_3$, the orbital ordering is confirmed by the resonant elastic x-ray scattering below $T_L = 140\text{K}$, and the static Jahn-Teller distortion is released in this temperature range.¹¹ Therefore, the low lying excitation is expected to be observed without disturbance of the lattice distortion. In the spin canted phase among the above two concentration region, the anisotropy of the spin correlation function decreases and the gap in the orbital excitation gradually decreases with doping holes. Such kind of control of the orbital excitation is possible by changing the spin structure in the magnetic field.

As a probe to detect the orbital excitation, we propose the two possible methods by using the inelastic resonant x-ray scattering. In the present case, the dispersion relation is detectable due to the smaller wave length of the x-ray in comparison with the conventional light (the wave lengths in the L- and K-edge cases are about 2.1\AA and 19.6\AA , respectively). In the L-edge case, the orbital excitation is directly caused by $2p \rightarrow 3d$ transition and the single orbital wave without the spin flipping is only brought about. In the spin-F case with orbital $(\theta/\theta + \pi)$, each mode of the orbital wave is separately observed by choosing the reciprocal lattice vector \vec{G} . This selection rule between the reciprocal lattice vector and the modes of the orbital wave is mainly due to the fact that the inelastic part of the scattering matrix is represented by the x component of the pseudo spin operator. Since the large scattering intensity is expected in the low energy region near the orbital superlattice reflection point, it may be observed without disturbance of the large fundamental elastic peak. The polarization dependence is remarkable, since it directly comes from the coupling constant between electron and photon. In the K-edge case, where the elastic scattering has already been used to observe the orbital ordering, the orbital excitation occurs through the screening process of the core hole. This process through the charge transfer from one of the nearest neighboring Mn ions is more favorable in manganites rather than in cuprates and nickelates, since the manganites are closer to the boundary between the charge transfer insulator and the Mott one. The one and two orbital wave excitations are possible in the same order, unlike the conventional two magnon Raman scattering. The orbital excitation occurs in the site where the x-ray excites the $1s$ electron and its one of the nearest neighboring Mn sites. Owing to the unique excitation process, the structure factor shows the strong momentum dependence and in particular the intensity vanishes around the Γ -point. Through the measurement of the characteristic momentum dependence, it is possible to identify the orbital sector in the inelastic component and the mechanism of the orbital excitation proposed in this paper.

ACKNOWLEDGEMENTS

The authors would like to thank Y. Endoh, Y. Murakami and J. Mizuki for their valuable discussions. We also indebted to M. Kaji and S. Okamoto for their helpful discussions and calculations. This work was supported by Priority Areas Grants from the Ministry of Education, Science and Culture of Japan, CREST (Core Research for Evolutional Science and Technology Corporation) Japan, and NEDO Japan. Part of the numerical calculation was performed in the HITACS-3800/380 supercomputing facilities in Institute for Materials Research, Tohoku University.

APPENDIX A: ELASTIC SCATTERING IN THE L-EDGE CASE

In this appendix, we introduce the elastic x-ray scattering in the L-edge case as a method to detect the orbital order. We focus on the polarization and orbital dependence of the atomic scattering factor in the orbital ordered phase. Once the dependence is revealed, the scattering intensity in the several orbital ordering is obtained by the formulas in Ref. 14. The atomic scattering factor is calculated by the perturbational calculation presented in Sect. IIIA and given by

$$f_{i\alpha\alpha} = |A_{\gamma\theta-\alpha}^{(L)}|^2 \frac{3}{2} E^{(t)-1} + |A_{\gamma\theta-\alpha}^{(L)}|^2 \frac{1}{2} E^{(s)-1} + |A_{\gamma\theta\alpha}^{(L)}|^2 E^{(d)-1}. \quad (\text{A1})$$

As well as in the inelastic case, we approximately set up the state and the energy for the intermediate states in the scattering. We assume that the states consist of the following three states: $|t\underline{2p}_\alpha\rangle$, $|s\underline{2p}_\alpha\rangle$, and $|d_\gamma\underline{2p}_\alpha\rangle$, where $|s\rangle(|t\rangle)$ represents the state where two e_g electrons occupy the different orbital with the spin singlet (triplet) and $|d_\gamma\rangle$ is the doubly occupied state in the γ orbital. These energies are approximately estimated as $E^{(t)} = U' - J + \Delta + 2F_0(3d, 2p) - \omega_k + i\Gamma$ with $\Delta = \varepsilon_d - \varepsilon_p$, $E^{(s)} = U' + J + 2J_H + \Delta + 2F_0(3d, 2p) - \omega_k + i\Gamma$ and $E^{(d)} = U + 2J_H + \Delta + 2V(3d_\gamma, 2p_\alpha) - \omega_k + i\Gamma$, where Γ is the damping constant. Because $E^{(t)}$ is the smallest, $|t\underline{2p}_\alpha\rangle$ dominates the L-edge. It is noticed that the energy $E^{(t)}$ is independent of the occupied $3d$ orbital and the polarization of x-ray, because two e_g orbitals are occupied in the intermediate state and three $2p$ orbitals are occupied in the initial and final states. On the other hand, its intensity in Eq.(A1) is proportional to $|A_{\gamma\theta-\alpha}^{(L)}|^2$ which clearly depends on the occupied orbital and the polarization as shown in Eq.(27). It is concluded that the anisotropy of the scattering factor is originated from the coupling constant between electron and photon, unlike that in the K-edge case where the Coulomb interaction between $3d$ and $4p$ gives rise to the anisotropy.¹³ For example, In the antiferro-type orbital ordering, where two

kinds of the orbital sublattice exist, the scattering intensity at the orbital superlattice reflection is proportional to $|(A_{\gamma_{A-\alpha}}|^2 - |A_{\gamma_{B-\alpha}}|^2)|^2$, where $\gamma_{A(B)-}$ is the unoccupied orbital state in the A(B)-orbital sublattice.

APPENDIX B: DETAILED DERIVATION AND FORMULAS IN K-EDGE CASE

In this appendix, we present the detailed derivation and formulation of the effective Hamiltonian and transition probability in the K-edge case which are introduced in Sect. III B.

In derivation of the effective Hamiltonian, the unperturbed states are classified by the number of electron of Mn $3d$ and $4p$ orbitals at each site as $|n(3d), n(4p)\rangle$ and these states and energies are approximately set up as follows. The energy in $|1, 0\rangle$ is defined as the origin of the energy. $|1, 1\rangle$ consists of $|3d_\gamma^1 4p_\gamma^1 \underline{1s}\rangle$ and its energy is defined as $E_{11} = \Delta + V(3d_\gamma, 4p_\alpha) + V(3d, 1s) + V(4p, 1s) - \omega_k$ with $\Delta = \varepsilon_P - \varepsilon_s$. $|2, 0\rangle$ includes the three states represented by $|t\rangle$, $|s\rangle$ and $|d\rangle$, as we explained in Appendix A, with the energies $E_{20}^{(t)} = U' - J$, $E_{20}^{(s)} = U' + J + 2J_H$ and $E_{20}^{(d)} = U + 2J_H$, respectively. In the same way, $|2, 1\rangle$ consists of the three states: $|t 4p_\alpha^1 \underline{1s}\rangle$, $|s 4p_\alpha^1 \underline{1s}\rangle$ and $|d_\gamma 4p_\alpha^1 \underline{1s}\rangle$ with energies $E_{21}^{(t)} = U' - J + \Delta + 2F_0(3d, 4p) + V_{core} - \omega_k$, $E_{21}^{(s)} = U' + J + 2J_H + \Delta + 2F_0(3d, 4p) + V_{core} - \omega_k$ and $E_{21}^{(d)} = U + 2J_H + \Delta + 2V(3d_\gamma, 4p_\alpha) + V_{core} - \omega_k$, respectively, with $V_{core} = 2V(3d, 1s) + V(4p, 1s)$. In all states, the t_{2g} spin is assumed to be parallel to the e_g one and the spin dependence of the core hole interaction are neglected. Among these parameters, we choose the independent parameters $w_0 = 4F_2(4p, 3d)$, $W' = U + 2J + V(1s, 3d) + F_0(4p, 3d) - 5J$ and $\tilde{U} = U - 3J$ with $U' - J + \Delta + 2F_0(3d, 4p) + V_{core} - \omega_k = 0$, $V(1s, 3d) = V(1s, 4p)$ and $J = J_H$.

The matrix element of the effective Hamiltonian $(\tilde{H})_{ln}$ is derived by the conventional canonical transformation. The perturbational processes are characterized by the set of the initial, intermediate and final states: $(|l\rangle, |m\rangle, |n\rangle)$. In the calculation, $|n(3d), n(4p)\rangle = \{|1, 0\rangle, |2, 1\rangle\}$ are included explicitly and $\{|2, 0\rangle, |1, 1\rangle\}$ are introduced in the virtual senses. \tilde{H}_{3d} in Eq.(40) corresponds to the process $(|l\rangle, |m\rangle, |n\rangle) = (|1, 0\rangle, |2, 0\rangle, |1, 0\rangle)$. The effective electron-photon interaction \tilde{H}_{e-p} in Eq.(41) is derived by $(|2, 1\rangle, |2, 0\rangle|1, 0\rangle)$ and $(|2, 1\rangle, |1, 1\rangle, |1, 0\rangle)$. In this term, $\Gamma_{\gamma\alpha}^{(m)}$ is given by

$$\Gamma_{\gamma\alpha}^{(m)} = \frac{1}{2} \left((E_{21}^{(m)} - E_{11})^{-1} + (E_{10} - E_{11})^{-1} + (E_{21}^{(m)} - E_{20}^{(m)})^{-1} + (E_{10} - E_{20}^{(m)})^{-1} \right). \quad (\text{B1})$$

The second term H_{core} in Eq.(40) is derived by the process $(|2, 1\rangle, |1, 1\rangle, |2, 1\rangle)$ and its 0-th order term of the

perturbation is used in the calculation of the transition probability. The processes $(|1, 0\rangle, |1, 1\rangle, |1, 0\rangle)$ and $(|2, 1\rangle, |2, 0\rangle, |2, 1\rangle)$ imply the elastic off-resonance scattering and the higher order x-ray scattering, respectively, and these are irrelevant in the present scattering.

In the scattering matrix in Eq.(43), $D_\alpha^{(m)}$ is the energy denominator originated from the second order perturbational process of \tilde{H}_{e-p} and it is represented by

$$D_\alpha^{(m)} = (E_{21}^{(m)} - E_{10} + i\Gamma)^{-1}. \quad (\text{B2})$$

$I_{ij}^{(m)}$ in Eq.(43) describes the changes of the spin and orbital states defined as

$$I_{ij\alpha}^{(t)} = \left(\frac{3}{4} + \vec{S}_i \cdot \vec{S}_j \right) \times (\Gamma_{b\alpha}^{(t)2} \tau_{ij}^A + \Gamma_{a\alpha}^{(t)2} \tau_{ij}^B - \Gamma_{a\alpha}^{(t)} \Gamma_{b\alpha}^{(t)} \tau_{ij}^C), \quad (\text{B3})$$

$$I_{ij\alpha}^{(s)} = \left(\frac{1}{4} - \vec{S}_i \cdot \vec{S}_j \right) \times (\Gamma_{b\alpha}^{(s)} \tau_{ij}^A + \Gamma_{a\alpha}^{(s)2} \tau_{ij}^B + \Gamma_{a\alpha}^{(s)} \Gamma_{b\alpha}^{(s)} \tau_{ij}^C), \quad (\text{B4})$$

and

$$I_{ij\alpha}^{(d)} = 2 \left(\frac{1}{4} - \vec{S}_i \cdot \vec{S}_j \right) (\Gamma_{a\alpha}^{(d)2} \tau_{ij}^{A'} + \Gamma_{b\alpha}^{(d)2} \tau_{ij}^{B'}), \quad (\text{B5})$$

with

$$\tau_{ij}^A = n_{ib} (t_{ij}^{aa2} n_{ja} + t_{ij}^{ab2} n_{jb} + 2t_{ij}^{aa} t_{ij}^{ab} T_{jx}), \quad (\text{B6})$$

$$\tau_{ij}^B = n_{ia} (t_{ij}^{ba2} n_{ja} + t_{ij}^{bb2} n_{jb} + 2t_{ij}^{bb} t_{ij}^{ba} T_{jx}), \quad (\text{B7})$$

$$\tau_{ij}^C = 2 (t_{ij}^{aa} t_{ij}^{ba} T_{ix} n_{ja} + t_{ij}^{bb} t_{ij}^{ab} T_{ix} n_{jb} + 2t_{ij}^{aa} t_{ij}^{bb} T_{ix} T_{jx}), \quad (\text{B8})$$

$$\tau_{ij}^{A'} = n_{ia} (t_{ij}^{aa2} n_{ja} + t_{ij}^{ab2} n_{jb} + 2t_{ij}^{aa} t_{ij}^{ab} T_{jx}), \quad (\text{B9})$$

$$\tau_{ij}^{B'} = n_{ib} (t_{ij}^{ba2} n_{ja} + t_{ij}^{bb2} n_{jb} + 2t_{ij}^{bb} t_{ij}^{ba} T_{jx}). \quad (\text{B10})$$

The coefficients $B_{\nu\delta}^{(m)}$ and $C_{\nu\delta}^{(m)}$ in Eq. (44) are obtained by taking the average for the spin part as

$$C_{\nu\nu'}^{(t)} = - \left(\frac{3}{4} + \langle \vec{S}_\nu \cdot \vec{S}_{\nu'} \rangle \right) \Gamma_{a\alpha}^{(t)} \Gamma_{b\alpha}^{(t)} t_{\nu\nu'}^{aa} t_{\nu\nu'}^{ba}, \quad (\text{B11})$$

$$C_{\nu\nu'}^{(s)} = \left(\frac{1}{4} - \langle \vec{S}_\nu \cdot \vec{S}_{\nu'} \rangle \right) \Gamma_{a\alpha}^{(s)} \Gamma_{b\alpha}^{(s)} t_{\nu\nu'}^{aa} t_{\nu\nu'}^{ba}, \quad (\text{B12})$$

$$C_{\nu\nu'}^{(d)} = 0, \quad (\text{B13})$$

$$B_{\nu\nu'}^{(t)} = \left(\frac{3}{4} + \langle \vec{S}_\nu \cdot \vec{S}_{\nu'} \rangle \right) \Gamma_{a\alpha}^{(t)2} t_{\nu\nu'}^{bb} t_{\nu\nu'}^{ba}, \quad (\text{B14})$$

$$B_{\nu\nu'}^{(s)} = \left(\frac{1}{4} - \langle \vec{S}_\nu \cdot \vec{S}_{\nu'} \rangle \right) \Gamma_{\alpha\alpha}^{(s)2} t_{\nu\nu'}^{bb} t_{\nu\nu'}^{ba} , \quad (\text{B15})$$

and

$$B_{\nu\nu'}^{(d)} = 2 \left(\frac{1}{4} - \langle \vec{S}_\nu \cdot \vec{S}_{\nu'} \rangle \right) \Gamma_{\alpha\alpha}^{(d)2} t_{\nu\nu'}^{aa} t_{\nu\nu'}^{ab} . \quad (\text{B16})$$

-
- ¹ K. Chahara, T. Ohono, M. Kasai, Y. Kanke, and Y. Kozono, *Appl. Phys. Lett.* **62**, 780 (1993).
- ² R. von Helmolt, J. Wecker, B. Holzapfel, L. Schultz, and K. Samwer, *Phys. Rev. Lett.* **71**, 2331 (1993).
- ³ Y. Tokura, A. Urushibara, Y. Moritomo, T. Arima, A. Asamitsu, G. Kido, and N. Furukawa, *Jour. Phys. Soc. Jpn.* **63**, 3931 (1994).
- ⁴ S. Jin, T. H. Tiefel, M. McCormack, R. A. Fastnacht, R. Ramesh, and L. H. Chen, *Science* **264**, 413 (1994).
- ⁵ J. B. Goodenough, *Phys. Rev.* **100**, 564 (1955).
- ⁶ J. Kanamori, *J. Phys. Chem. Solids* **10**, 87 (1959).
- ⁷ K. I. Kugel and D. I. Khomskii, *JETP Lett.* **15**, 446 (1972).
- ⁸ Y. Ito, and J. Akimitsu, *Jour. Phys. Soc. Jpn.* **40**, 1333 (1976).
- ⁹ Y. Murakami, H. Kawada, H. Kawata, M. Tanaka, T. Arima, H. Moritomo and Y. Tokura, *Phys. Rev. Lett.* **80**, 1932 (1998).
- ¹⁰ Y. Murakami, J. P. Hill, D. Gibbs, M. Blume, I. Koyama, M. Tanaka, H. Kawata, T. Arima, T. Tokura, K. Hirota, and Y. Endoh, *Phys. Rev. Lett.* **81**, 582 (1998),
- ¹¹ Y. Endoh, K. Hirota, N. Nojiri, T. Fukuda, K. Kaneko, H. Kimura, Y. Murakami, S. Okamoto, S. Ishihara, and S. Maekawa, (unpublished).
- ¹² K. Nakamura, T. Arima, A. Nakazawa, Y. Wakabayashi, and Y. Murakami, (unpublished).
- ¹³ S. Ishihara, and S. Maekawa, *Phys. Rev. Lett.* **80**, 3799 (1998),
- ¹⁴ S. Ishihara, and S. Maekawa, *Phys. Rev. B* **58**, 13449 (1998).
- ¹⁵ M. Fabrizio, M. Altarelli, and M. Benfatto, *Phys. Rev. Lett.* **80**, 3400 (1998).
- ¹⁶ M. Cyrot, and C. Lyon-Caen, *Le Jour. de Physique* **36**, 253 (1975).
- ¹⁷ S. Ishihara, J. Inoue, and S. Maekawa, *Physica C* **263**, 130 (1996), and *Phys. Rev. B* **55**, 8280 (1997).
- ¹⁸ J. van den Brink, W. Sekelenburg, D. I. Khomskii, and G. A. Sawatzky, *Phys. Rev. B* **58**, 10276 (1998).
- ¹⁹ S. Ishihara, M. Yamanaka, and N. Nagaosa, *Phys. Rev. B* **56**, 686 (1997).
- ²⁰ J. Inoue, S. Okamoto, S. Ishihara, W. Koshibae, Y. Kawamura, and S. Maekawa. *Physica B* **237-238**, 51 (1997) .
- ²¹ P. M. Platzman, and E. D. Isaacs, *Phys. Rev. B* **57**, 11107 (1998), and *Raman Emission by X-ray Scattering*, edited by D. L. Ederer, and J. H. McGuire. World Scientific, Singapore, (1996).
- ²² P. Kuiper, J. -H. Guo, C. Sathel, L. -C. Duda, J. Nordgren, J. J. M. Poethuizen, F. M. F. de Groot, and G. A. Sawatzky, *Phys. Rev. Lett.* **80**, 5204 (1998).
- ²³ J. P. Hill, C. -C. Kao, W. A. L. Caliebe, M. Matsubara, A. Kotani, J. L. Peng, and R. L. Greene, *Phys. Rev. Lett.* **80**, 4967 (1998).
- ²⁴ R. Maezono, S. Ishihara, and N. Nagaosa, *Phys. Rev. B* **57**, R13993 (1998).
- ²⁵ R. Shiina, T. Nishitani and H. Shiba, *J. Phys. Soc. Jpn.* **66**, 3159 (1997).
- ²⁶ G. Khaliullin, and V. Oudovenko, *Phys. Rev. B* **56**, R14243 (1998).
- ²⁷ L. F. Feiner, A. M. Oles, and J. Zaanen, (unpublished) cond-mat/9805203.
- ²⁸ J. van den Brink, P. Horsch, F. Mack, and A. M. Oles, (unpublished).
- ²⁹ J. M. Tranquada, S. M. Heald, W. Kunnmann, A. R. Moodenbaugh, S. L. Qiu, Y. Xu, and P. K. Davies, *Phys. Rev. B.* **44**, 5176 (1991).
- ³⁰ A. Sahiner, M. Croft, S. Guha, I. Perez, Z. Zhang, M. Greenblatt, P. A. Metcalf, H. Jahns, and G. Liang, *Phys. Rev. B.* **51**, 5879 (1995).
- ³¹ T. Arima, Y. Tokura, and J. B. Torrance, *Phys. Rev. B* **48**, 17006 (1993), A. E. Bocquet, T. Mizokawa, K. Morikawa, A. Fujimori, S. R. Barman, K. Maiti, D. D. Sarma, Y. Tokura, and M. Onoda, *Phys. Rev. B* **53**, 1161 (1996).

Figure captions

FIG. 1. The mean field phase diagram at zero temperature. F , A , C , and G imply the ferromagnetic structure, and the layer-type, rod-type and NaCl-type antiferromagnetic structures, respectively.

FIG. 2. The dispersion relation of the orbital wave in the spin-F case. The Brillouin zone for the face-centered cubic lattice is adopted. The orbital states for the two orbital sublattices are denoted by $(\theta_A/\theta_A + \pi)$.

FIG. 3. The dispersion relation of the orbital wave in the spin-A case. The Brillouin zone for the tetragonal lattice is adopted. $J_2/J_1 = 0.5$ which corresponds to the orbital state (θ_A/θ_A) with $\theta_A = 1.34$. μ denotes the mode of the orbital wave.

FIG. 4. The schematic picture of the orbital excitation processes in (a) the L-edge case and (b) the K-edge case. j denotes one of the nearest neighbor sites of i . The broken arrows indicate the incident and scattered x-rays.

FIG. 5. The square of the structure factor for the orbital wave with spin-F in the L-edge case: $I_L = |F_{\mu\alpha}(\vec{q}, \vec{G})|^2 / (D|A_0|^2)^2$. (a) $h + k + l = \text{even}$, and (b) odd where (h, k, l) is defined in a unit cell in the face-centered cubic lattice. The orbital state is chosen as $(\frac{\pi}{2}/\frac{\pi}{2} + \pi)$. The shaded circles and squares mean the x and z polarization cases, respectively.

FIG. 6. The square of the structure factor for the orbital wave with spin-A in the L-edge case: $I_L = |F_{\mu\alpha}(\vec{q}, \vec{G})|^2 / (D|A_0|^2)^2$. (a) $h + k = \text{even}$ and $l = \text{odd}$, and (b) $h + k = \text{odd}$ and $l = \text{odd}$, where (h, k, l) is defined in a unit cell in the tetragonal lattice. $J_2/J_1 = 0.5$ which corresponds to the orbital state (θ_A/θ_A) with $\theta_A = 1.34$. The polarization is parallel to the x -direction. The open and filled circles mean (a) the $(+-)$ - and $(-+)$ -modes, and (b) the $(--)$ - and $(++)$ -modes, respectively.

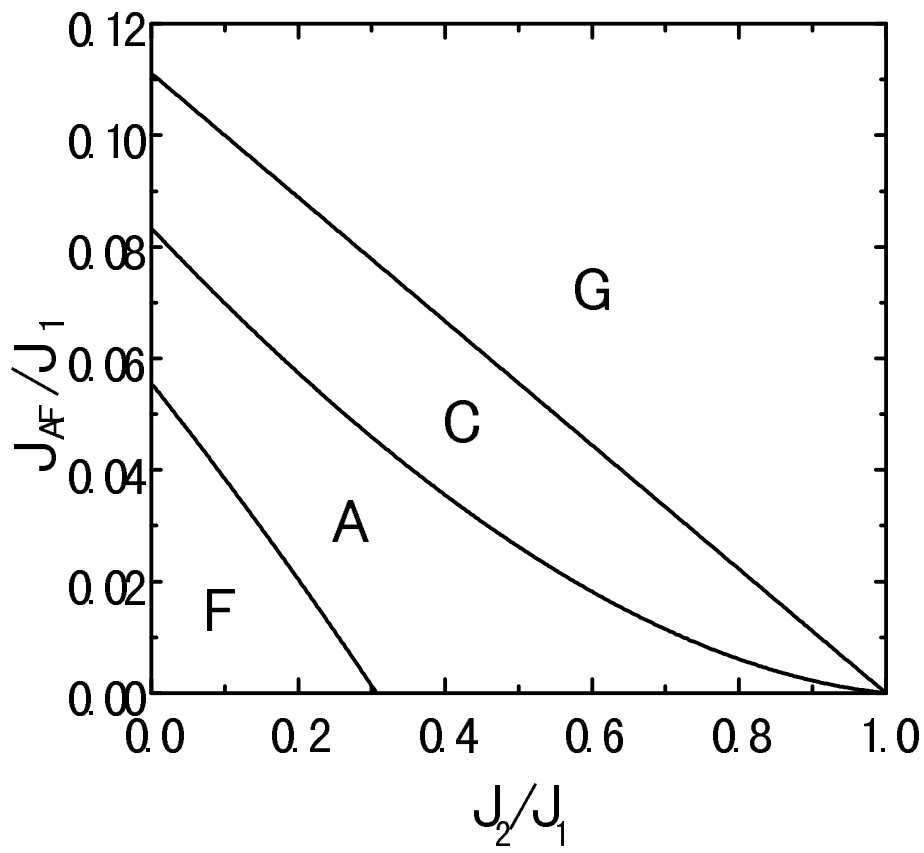
FIG. 7. The schematic picture of the excitation process of the one orbital wave in the K-edge case. j denotes one of the nearest neighbor sites of i where $1s \rightarrow 4p$ transition is caused by x-ray. The two levels indicate the degenerate e_g orbitals. The straight and broken arrows indicate the first and second electronic processes in the scattering, respectively.

FIG. 8. The square of the structure factor for the orbital wave with spin-F in the K-edge case: $I_K = |F_{\mu\alpha}(\vec{q}, \vec{G})|^2 / (2t_0^{-1}|A^{(K)}|^2)^2$. (a) $h + k + l = \text{even}$, and (b) odd where (h, k, l) is defined in a unit cell in the face-centered cubic lattice. The orbital state is chosen as $(\frac{\pi}{2}/\frac{\pi}{2} + \pi)$. The polarization is parallel to the x -direction. The open and filled circles mean the $(-)$ - and $(+)$ -modes, respectively.

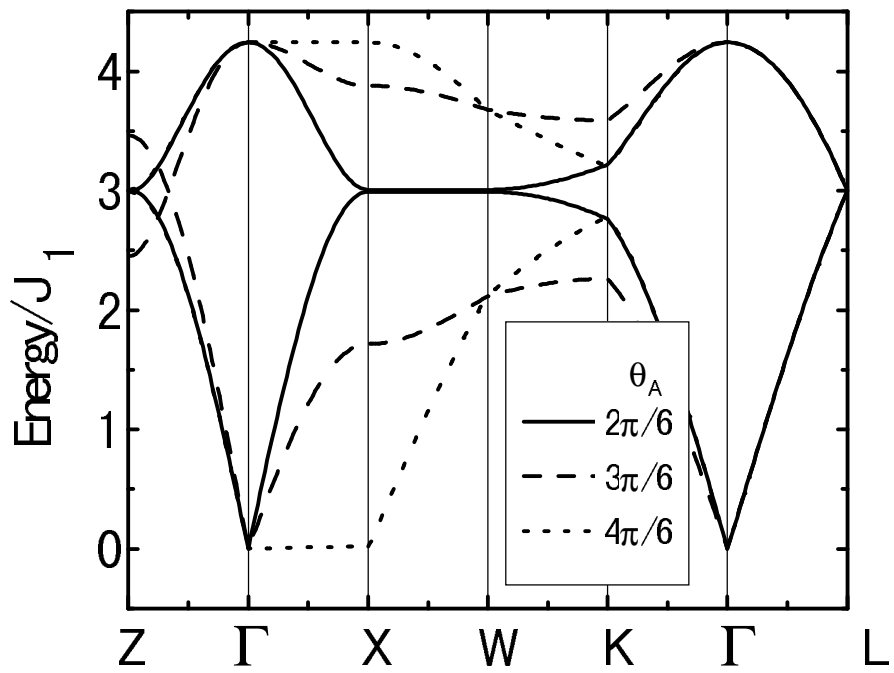
Fig. 9 The polarization dependence of the square of the structure factor for the orbital wave $((+)$ -mode) with spin-F in the K-edge case. (a) $h + k + l = \text{even}$, and (b) odd

where (h, k, l) is defined in a unit cell in the face-centered cubic lattice.

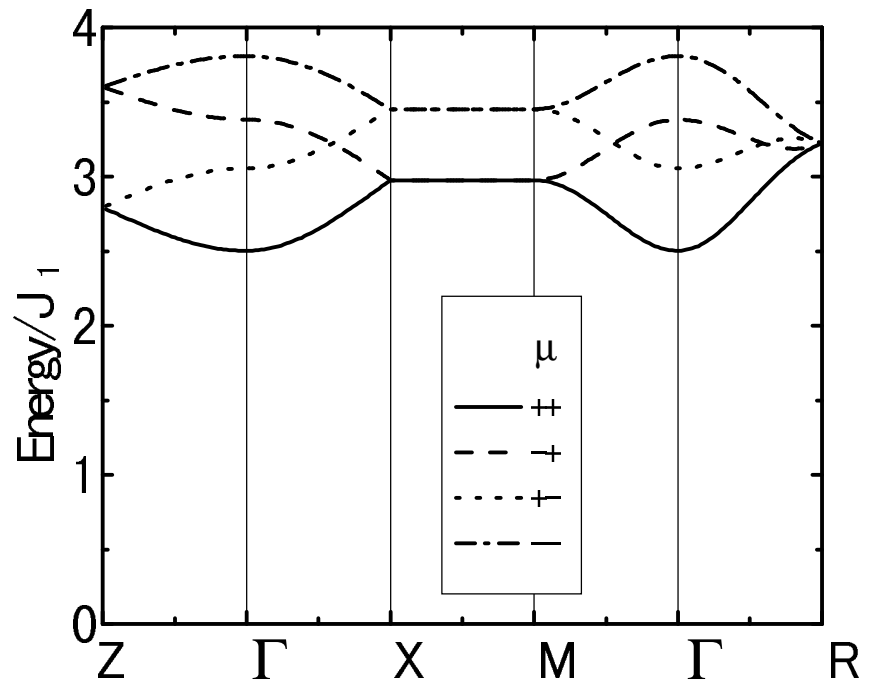
FIG. 10. The square of the structure factor for the orbital wave with spin-A in the K-edge case: $I_K = |F_{\mu\alpha}(\vec{q}, \vec{G})|^2 / (2t_0^{-1}|A^{(K)}|^2)^2$. (a) $h + k = \text{even}$ and $l = \text{odd}$, and (b) $h + k = \text{odd}$ and $l = \text{odd}$, where (h, k, l) is defined in a unit cell in the tetragonal lattice. $J_2/J_1 = 0.5$ which corresponds to the orbital state (θ_A/θ_A) with $\theta_A = 1.34$. The polarization is parallel to the x -direction. The open and filled circles mean (a) the $(+-)$ - and $(-+)$ -modes, and (b) the $(--)$ - and $(++)$ -modes, respectively.



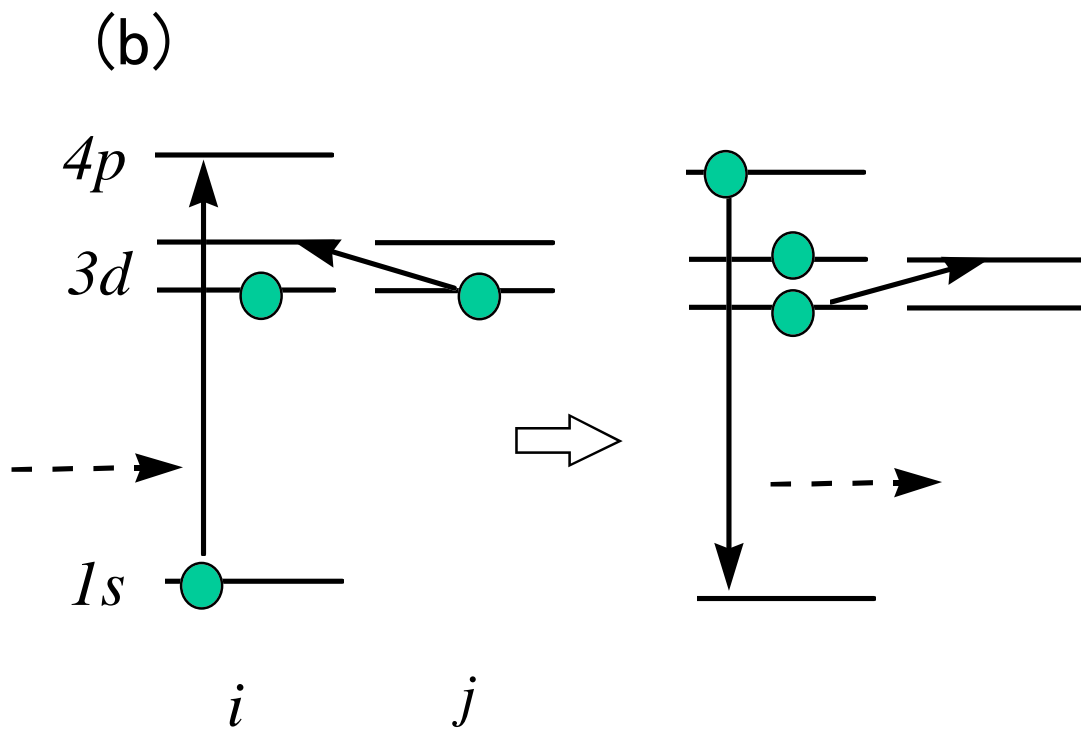
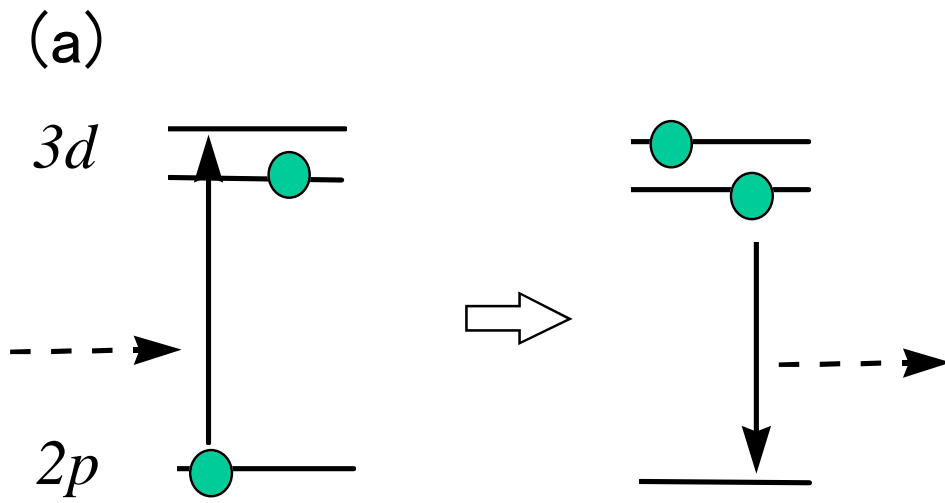
Ishihara et al. Fig.1



Ishihara et al. Fig. 2

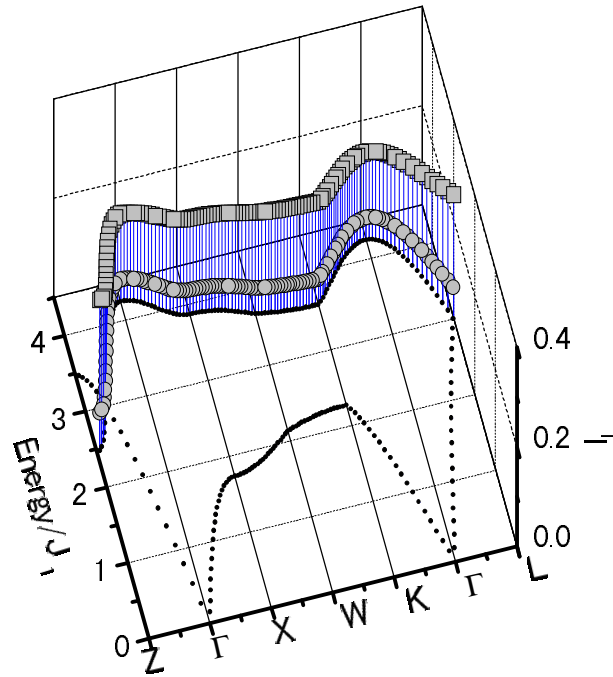


Ishihara et al. Fig. 3

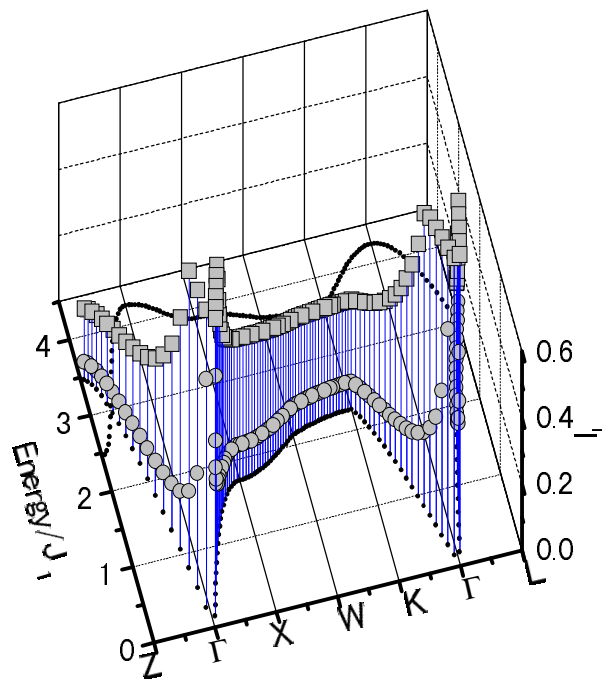


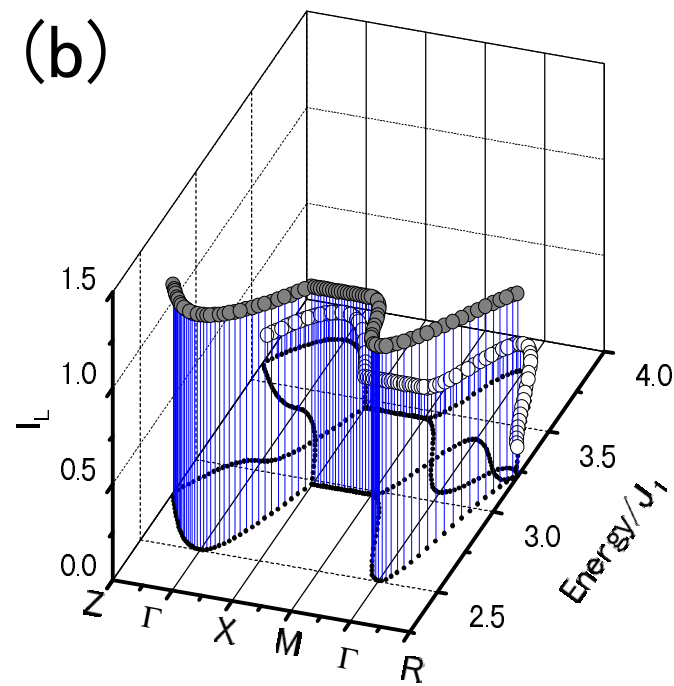
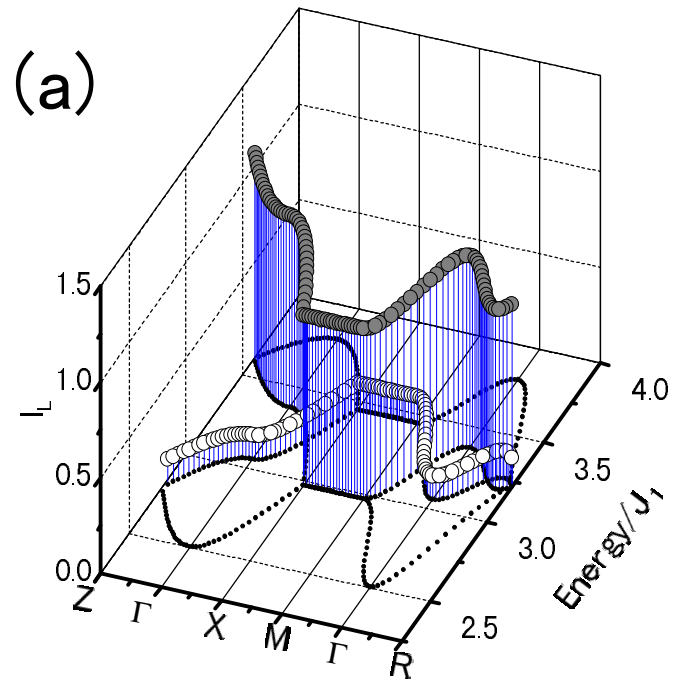
Ishihara et al. Fig. 4

(a)

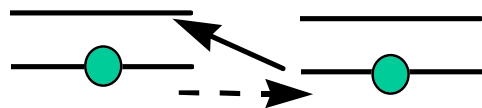


(b)

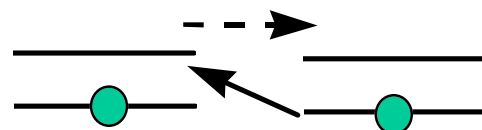




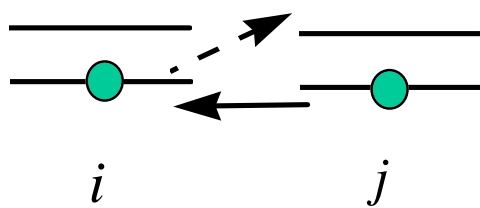
(a)



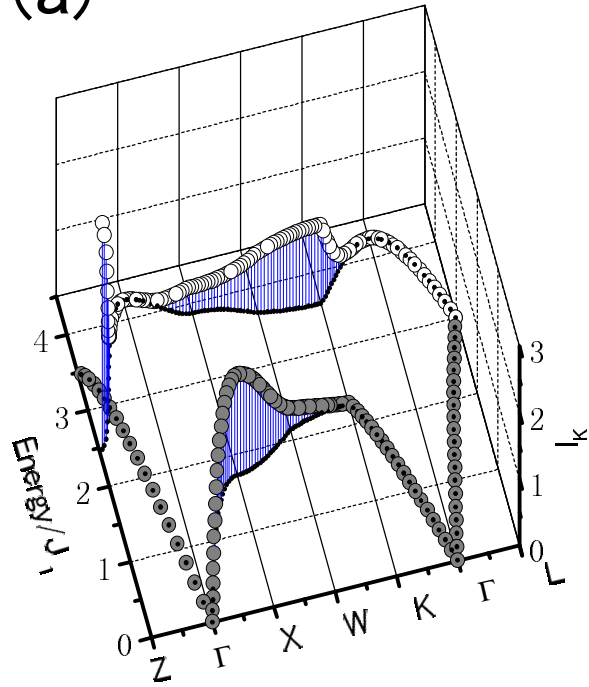
(b)



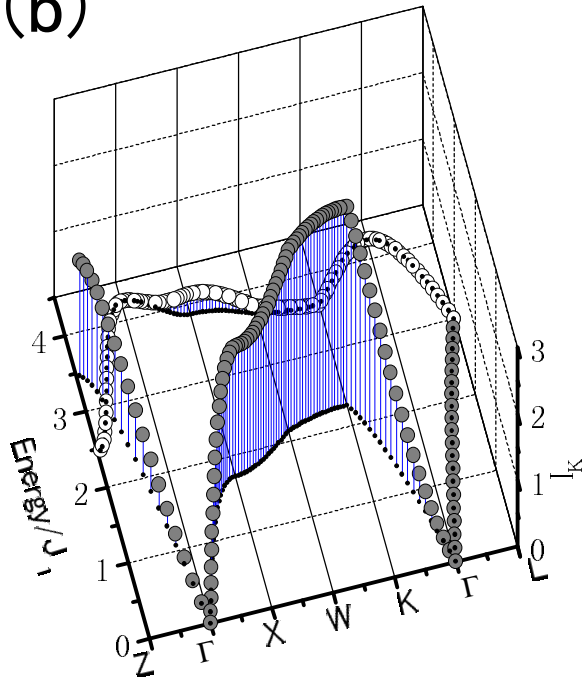
(c)

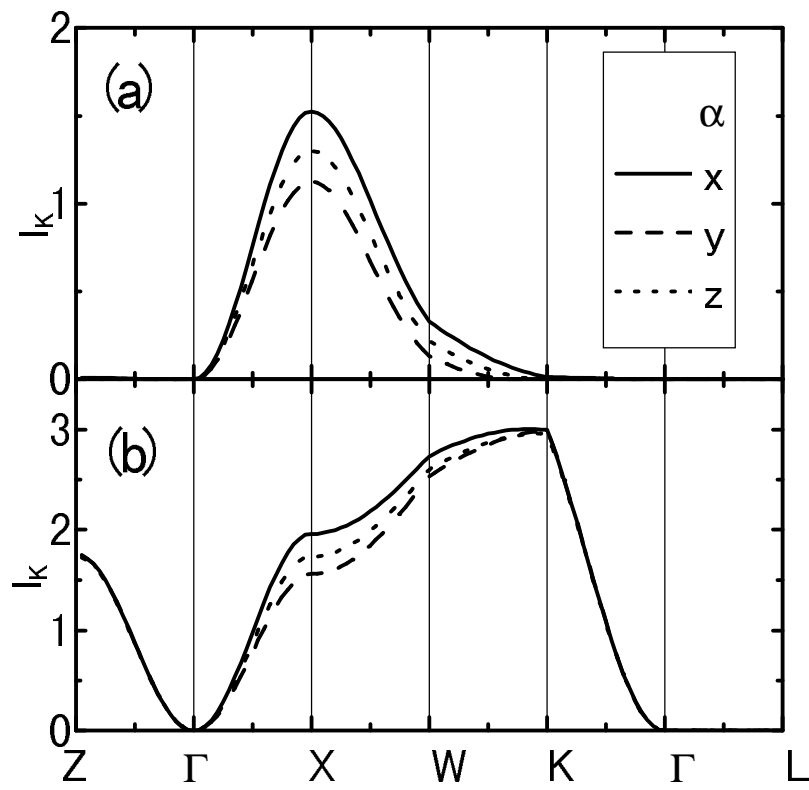


(a)



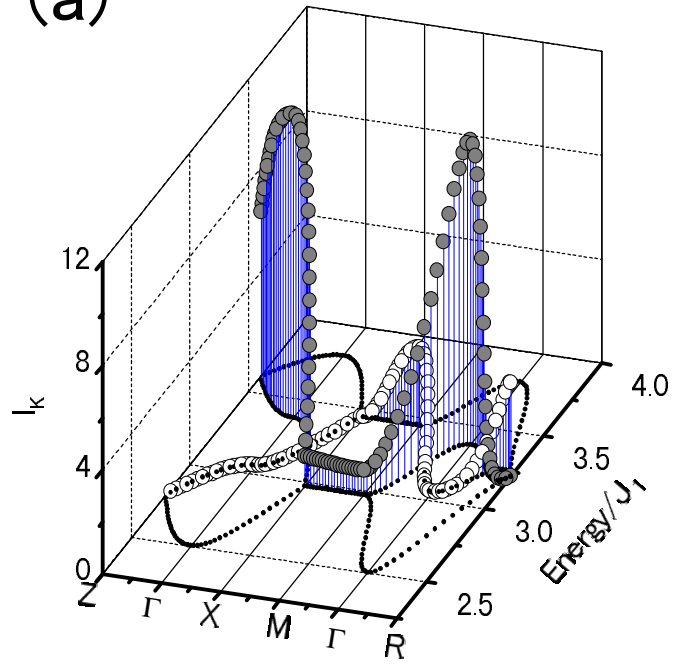
(b)





Ishihara et al. Fig. 9

(a)



(b)

